J. Condensed Matter Nucl. Sci. 14 (2014) 29–49

Research Article

The Use of CR-39 Detectors in LENR Experiments

P.A. Mosier-Boss*
Research Laboratory of Electronics, Massachusetts Institute of Technology, Cambridge, MA 02139, USA

L.P.G. Forsley
JWK International Corp., Annandale, VA 22003, USA

P.J. McDaniel
University of New Mexico, Albuquerque, NM 87131, USA

Abstract

In this communication, the use of CR-39 detectors to detect energetic charged particles and neutrons in LENR experiments is discussed. The main advantages of these detectors over real-time electronic detectors are its integration capability and its ability to speciate energetic particles. Unlike real-time detectors, CR-39 can be placed in close proximity to the cathode and can be used for both electrolysis experiments and gas loading. These advantages of CR-39 detectors over real time, electronic detectors are particularly important when energetic particle emissions occur either sporadically in bursts or at a low flux.
 ISSN 2227-3123

Keywords: Charged particles, CR-39, Neutrons, Real-time electronic detectors

1. Introduction

Columbia Resin 39 (CR-39) is an allyl glycol carbonate plastic that is optically clear and amorphous. In 1978, Cartwright et al. [1] were the first to show that CR-39 could be used to detect nuclear particles. As an energetic, charged particle traverses through the plastic, it creates along its path an ionization trail that is more sensitive to chemical etching than the bulk material. After etching with an aqueous 6 M NaOH solution between 60 and 70°C for six or more hours, tracks due to the energetic particles remain in the form of pits that can be examined with the aid of an optical microscope. As will be discussed in this communication, the size, depth of penetration, and shape of the track provides information about the mass, charge, energy, and direction of motion of the particle that created the track [2].

Since its introduction as a solid state nuclear track detector (SSNTD), CR-39 has found extensive use as a charged-particle spectrometer to study inertial-confinement-fusion (ICF) plasma [3] and to detect secondary neutrons and cos-

*E-mail: pboss@san.rr.com

 ISSN 2227-3123

Table 1. Summary of LENR Experiments Using CR-39.[a]

Researcher	Experiment	Conclusions
X.Z. Li et al. [5]	D_2 (H_2) gas loading of Pd foils	Track density: Pd/D_2 >>>> Pd/H_2 > D_2
Jin et al. [6]	D_2 gas loading of YBCO pellets and powder	Circular tracks with diameters between 2 and 7 μm (for comparison ^{241}Am α tracks have a diameter of 6 μm)
Lipson et al. [7]	Electrochemically load Au/Pd/PdO heterostructures with D. Once loaded put cathode in contact with CR-39 and cycle temperature	Detected tracks consistent with 2.5–3.0 MeV p and 0.5–1.5 MeV t
Roussetski [8]	Electrochemically load Au/Pd/PdO and PdO/Pd/PdO heterostructures with D. Once loaded put cathode in contact with CR-39 and cycle temperature	Detected tracks consistent with $\sim$3.0 MeV p, $\sim$1 MeV t, triple tracks due to 14.1 MeV n. The number of tritons needed to create triple tracks greater than the yield of DD tritons.
Karabut et al. [9]	Glow discharge of Ti cathodes in D_2 gas. CR-39 detectors covered in Al foils	Detected 3 MeV p, 1.7 MeV p or 2.3 MeV d, and 13.5$\pm$2.0 MeV α
Oriani and Fisher [10]	Pd sheet foil, electrolysis in Li_2SO_4/D_2O, CR-39 placed above and below Pd cathode	Track density of CR-39 used is electrolysis experiments (150–3760 tracks cm^{-2}) greater than CR-39 used in controls (59–541 tracks cm^{-2})
Lipson et al. [11]	Cathode was 50 μm thick Pd foil in contact with CR-39. Electrolysis in Li_2SO_4/H_2O	Tracks were concentrated in areas where the cathode was in contact with the CR-39 detector
Lipson et al. [12]	Cathode was thin Pd films in contact with CR-39. Cu and Al spacers separated the Pd cathode from the detector. Electrolysis in Li_2SO_4/H_2O	Tracks in CR-39 detectors consistent with 1.7 MeV p and 11–16 MeV α
Roussetski et al. [13]	Irradiate $TiH_x$and TiD_xfilms with psec laser beam. CR-39 in chamber either bare or covered with Al or Cu films	Detected 3 MeV p, n, and $\geq$10 MeV α
Lipson et al. [14]	TiD_x and Pd/PdO:D_x targets stimulated with a electron beam. Target surrounded by CR-39 covered with various metal foils	Detected 3 MeV p and 11–20 MeV α
Mosier-Boss et al. [15-18]	Pd/D codeposition on Ni screen and Ag, Au, Pt wires in contact with CR-39. Electrolysis in D_2O and H_2O	Detected tracks due to energetic charged particles and triple tracks due to 14.1 MeV n. Track density: D_2O >>>> H_2O
Tanzella et al. [19]	Pd/D codeposition on Ag wire in contact with CR-39 covered with either 6 μm Mylar or 60 μm polyethylene	Detected tracks due to 3 MeV p, 2.5 MeV n, 12.6–17.5 MeV p, 14.1 MeV n, and $\geq$ 12 MeV α

[a] p = proton, t = triton, d = deuteron, n = neutron, α = alpha

mic rays at the international space station (ISS) [4]. This detector has also been used in a number of low-energy nuclear reaction experiments for over two decades. These experiments and their results are summarized in Table 1. As shown in Table 1, these detectors have been used in gas phase experiments as well as electrolysis and glow discharge experiments. Hydriding materials used include Pd, Ti, Pd/PdO heterostructures, and YBCO. Energetic particles detected in LENR experiments include protons, alphas, tritons, and neutrons.

Lately, there has been much discussion on the validity of using SSNTDs in place of electronic, real-time detectors in LENR experiments. It has been argued that SSTNDs are a relatively new detector material whose use has not been fully vetted by the scientific community. In this communication, we indicate that the physics community has indeed fully evaluated and characterized SSNTDs such as CR-39 for energetic particle detection. We also discuss the advantages and disadvantages of SSNTDs and show that these detectors are not only ideal but are, in many cases, the detector of choice for use in LENR experiments to elucidate the nuclear nature of the phenomenon.

2. Overview of Real-time Methods to Detect Neutrons and Charged Particles

2.1. Neutron detection

Neutrons have no charge. Consequently, these particles cannot be detected directly. Instead indirect methods are used. In these methods, the neutrons interact with other atomic nuclei and it is the response of that interaction that is detected. In general, there are two categories of neutron interaction with other atomic nuclei. These are neutron capture or elastic scattering. In the neutron capture method, a target nucleus captures a neutron to create an unstable nucleus. This unstable nucleus then spontaneously loses energy by either emitting ionizing charged particles or gamma/X-rays. These are the decay products that are then detected. Because the cross sections for neutron capture are lower at high neutron energies, moderators are typically used to slow down the neutrons so that capture can occur. As a result, the energy of the neutron cannot be determined by this method. Neutron detectors that rely upon neutron capture include BF_3 and ^{3}He detectors. The efficiencies of these detectors for fast neutrons are of the order of 7.6×10^{-3} when in direct contact with the source [19]. The efficiency decreases with d^2, where d is the distance between the source and the detector. Srinivasen et al. [20] used three BF_3 counters embedded in a paraffin moderator block to monitor neutron emissions from a commercial Milton Roy diffusion type hydrogen generator. The cathode was comprised of 16 $Pd_{0.75}Ag_{0.25}$ straws that were 3 mm OD and 200 mm in length. The total surface area was 301 cm^2, much larger than is typically used in most LENR experiments. Neutrons were observed to occur in bursts. De Ninno et al. [21,22] used a BF_3 detector to monitor deuterium gas loading of 100 g of Ti shavings. Changes in temperature and pressure were used to create nonequilibrium conditions in adsorption/desorption of deuterium in the lattice. Neutron emissions were observed to occur in bursts that were between 35 and 500 times above background.

In the elastic scattering method, the neutron scatters off nuclei causing the struck nucleus to recoil. The recoiling nucleus can ionize and excite additional atoms through collisions. These collisions produce charge and/or scintillation light which are then detected. Since these types of detectors do not require moderators, the energy of the neutrons can be determined. However, these detectors also respond to gamma and X-rays. Consequently, a pulse-shape analyzer is required to differentiate neutrons of a given energy from gamma/X-rays. An example of a neutron detector that relies upon elastic scattering is the NE-213 liquid-scintillation detector. This detector was used by Lipson et al. [7] to measure neutron emissions from their Au/Pd/PdO:D heterostructures during exothermic deuterium desorption. To decrease the natural neutron background, the detectors were surrounded by boron-containing polyethylene, and the entire setup was placed in the underground laboratory of Hokkaido University under 10 m of heavy concrete. Because the efficiencies of these detectors to detect neutrons were on the order of 5%, Lipson et al. were able to measure 2.45 MeV neutrons at a count rate of $(19 \pm 2) \times 10^{-3}$n s^{-1} in a 4π solid angle. Srinivasen et al. [20] also used high recoil type plastic scintillator NE102A to monitor their Milton Roy hydrogen generators. In their experiments, the proton recoil counter tracked the BF_3 counters.

Jones et al. [23] used a neutron detector comprised of an outer ring of 16 ^{3}He-filled proportional counter tubes embedded in a polyethylene moderator and an inner ring of a plastic scintillating neutron detector viewed by a PMT to detect fast neutrons. A stainless steel sample chamber was placed inside the inner ring. Both gas loading and electrolytic loading of Ti foils were done. Neutron emissions were observed for the D_2 and D_2SO_4/D_2O systems but not for the corresponding H_2 and H_2SO_4/H_2O systems.

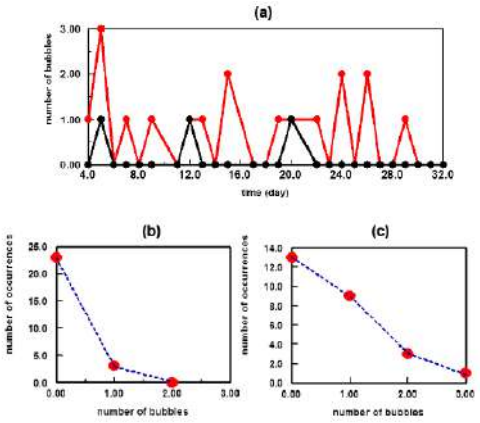

Figure 1. (a) Bubble detector results where red is for the cell and black is the background. Measurements began after the Pd was plated out. Summary of probability analysis done for (b) background (correlation = 0.99993) and (c) cell (correlation = 0.99964). Data points are indicated by (red filled circles) and calculated by (blue dotted line).

Bubble detectors are quasi-real-time neutron detectors. Tiny droplets of superheated liquid are dispersed throughout a clear moderating polymer inside the clear housing of the detector. When a thermalized neutron strikes a droplet and interacts with ^{6}Li, the droplet immediately vaporizes, forming a visible gas bubble trapped in the gel. The number of droplets provides a direct measurement of the tissue-equivalent neutron dose. The bubbles in the detector can be compressed and the detector can be reused for up to three months. Shyam and Rout [24] used an array of bubble detectors to detect neutrons created by imploding palladium deuteride X pinches using a low energy capacitor bank. The $PdD_{0.5}$ X pinches emitted 5×10^4 neutrons per discharge. Bubble detectors were used in a Pd/D co-deposition experiment on Ni screen. The bubble detector results are summarized in Fig. 1. It can be seen that more bubbles were seen for bubble detectors near the cell than were observed for the background (Fig. 1a). Probability analysis was used to analyze the data. The results for the cell and background are summarized in Fig.1b and c. From the analysis, the average number of neutrons per day for the cell was $69,200 \pm 6600$ and the background was $12,600 \pm 3300$. By paired *t*-test, the probability that the bubble detector results are random is one in a thousand. This indicates high statistical significance between the experiment and background. The neutron emission rate for the cell was estimated to be 0.65 n/s.

2.2. Charged particles

Ionization detectors are commonly used to detect charged particles in real time. Ionization detectors include gaseous ionization detectors and semiconductor detectors. Gaseous ionization detectors use the ionizing effect of radiation upon a gas-filled sensor. If a particle has enough energy to ionize a gas atom or molecule, the resulting electrons and ions cause a current flow which can be measured. The basic design of these detectors is two electrodes separated by air or a special fill gas. Examples of gaseous ionization detectors are ionization chambers, proportional counter, and Geiger–Müller tube. While these detectors are robust and inexpensive, they respond to gamma radiation, X-rays, beta particles, as well as charged particles. No spectral information can be generated and there is no discrimination between radiation types. An example of detectors of this type used in LENR experiments is the Femto-tech tritium gauge used by Claytor et al. [25]. In these experiments, a number of palladium alloys were loaded with either deuterium or hydrogen under low energy plasma bombardment. Tritium production was only observed when deuterium gas was

used. It was observed that most of the alloys did not produce tritium. Only the PdRhCoB, PdCu, PdRh (0.1%) and PdB alloys produced tritium under these experimental conditions.

Surface-barrier detectors are an example of semiconductor nuclear detectors used to detect charged particles in real time. These detectors consist of a piece of semiconductor (Si or Ge) that has been doped with impurity atoms to form a p–n junction. A reverse bias voltage is applied to this junction to create a depletion region near the front of the device in which there are no free charge carriers. When a charged particle enters the detector it loses its energy by the creation of electron–hole pairs in the depletion region. This is similar to ionization in gases. It is these small ionization currents that are detected and measured. To detect charged particles during electrolysis, Taniguchi et al. [26] used electrolysis cells whose bottoms were comprised of thin foil cathodes. The cathodes used were either thin Pd foils or Pd layers deposited on either stainless steel or Cu foils. The backside of these cathodes was placed on top of a conventional silicon surface barrier (SSB) detector. Count rates above background were observed for electrolysis experiments done in D_2O but not for H_2O. Taking into account energy losses, they attributed the species giving rise to the increased count rates to 3.03 MeV protons. Lipson et al. [7] used an SSB detector to detect the emission of 2.5–3.5 MeV protons during exothermic deuterium desorption of Au/Pd/PdO:D heterostructures. These heterostructures were mounted on top of a heater in a vacuum chamber. The SSB detector was positioned above the Au/Pd/PdO:D heterostructure. They also detected the emission of long-range alphas (alphas with energies between 8 and 14 MeV) during exothermic deuterium desorption of Au/Pd/PdO:D heterostructures under a 10^{-1} Pa vacuum [27]. To detect these long range alphas, they used a SSB $\Delta E - E$ counter telescope comprised of a thin ΔE-detector ($h = 20\mu$m) and thick E-detector ($E = 100$ μm). A coincidence timing gate of 20 ns was used. The requirement of coincidence between ΔE and E detectors eliminated electromagnetic noise and enabled identification of the charged particle type.

Jones et al. [28] developed a dual plastic/glass scintillator system to detect charged particles emissions by Ti foils. This charged particle spectrometer incorporated a 76 μm thick plastic scintillator adhered onto a thicker glass scintillator which was glued onto the face of a 12.7 cm diameter PMT. In these experiments, an array of five Ti foils (total surface area 180 cm^2) were loaded with deuterium in the gas phase. Afterwards, these $TiD_{0.5-1.4}$ foils were placed on the surface of the detector. Joule heating was used to create non-equilibrium conditions. Using this

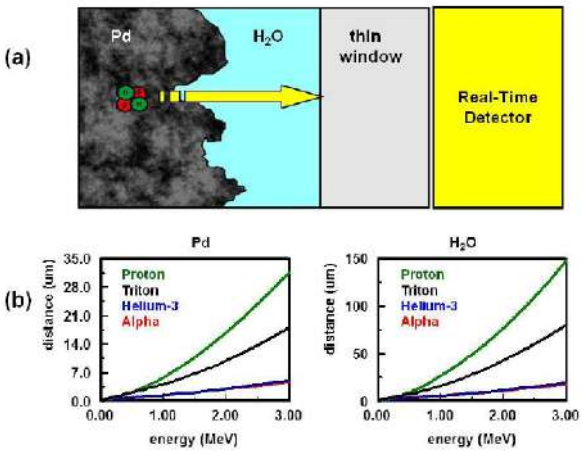

Figure 2. (a) Schematic describing the layers a charged particle has to negotiate before it reaches a real-time electronic detector. After its birth, a charged particle has to exit the metal lattice and cross a thin water layer and a thin window before it arrives at the detector. (b) LET curves calculated for charged particles traversing through palladium and water.

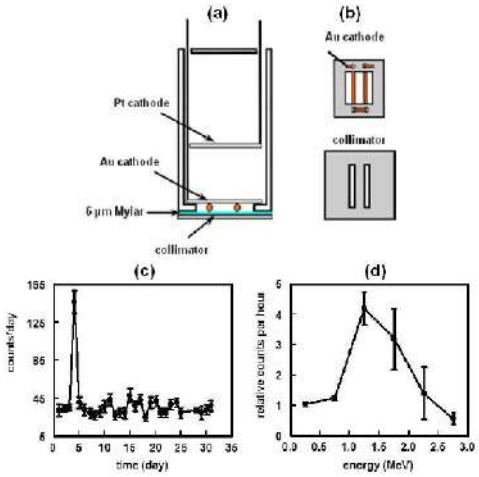

Figure 3. (a) Side view schematic of the cell used in the silicon surface barrier detector experiment. (b) Schematics of the Au-wire cathode and collimator used in the experiment. (c) Silicon barrier counts per day for the 1.0–1.5 MeV energy region. Arrow indicates when the current was turned on. (d) Relative counts per hour (day 4 count/day 3 bkg count) as a function of energy (MeV).

detector, they observed charged particle emissions in excess of 2000 counts per hour. Using an Al degrader between the $TiD_{0.5-1.4}$ foil and the plastic scintillator, they attributed those emissions to 3 MeV protons.

2.3. Problems with real-time detection methods

Many of the LENR experiments summarized in Table 1 involved electrolysis. Real-time, energetic particle detectors cannot be immersed in the cell. They have to be placed outside the cell. Since real-time detectors are positioned outside the cell, the likelihood of detection decreases by a factor of the square distance from the cathode. Consequently, these detectors have to be placed in close proximity to the cell and, in particular, the cathode. Figure 2a shows a schematic of the placement of a real-time detector next to a thin window that is in close proximity to a Pd cathode. A thin film of solution separates the cathode from the window. The emission of energetic particles from a source, i.e. cathode, occurs isotropically. The presence of the cathode, water film, and thin window will not impact neutrons. However, charged particles will experience energy losses as they traverse through the cathode, water film, and thin window to reach the detector. Linear energy transfer (LET) curves for charged particles traversing through Pd and water, Fig. 2b, were calculated using the SRIM-2003.26 code of Ziegler and Biersack [29]. These curves show that charged particles do not travel far through Pd metal and an aqueous medium.

Electronic particle detectors can be subject to low level electronic noise picked up from the local environment. For example, Jones et al. [30] retracted claims of neutron emissions from Pd/LiOD electrolytic cells when it was found that the large bursts they were seeing with their ^{3}He detectors were actually the result of high voltage breakdown in the electronics. The retraction was for the ^{3}He detector only and does not imply a retraction of highly-publicized earlier results and publications using the BYU neutron spectrometer nor the charged-particle spectrometer described above. Those results have not been retracted. Besides electronic noise, these real-time detectors are temperature sensitive. Also with real-time detectors, long acquisition times are typically used to improve the signal to noise ratio. If the rate of energetic particle production is sporadic and/or at a low level, the resultant signal can be averaged away when long acquisition times are used. Another problem with neutron detectors is multiplicity. If multiple neutrons hit the detector

Table 2. Estimated energies of charged particles emitted from the surface of the Pd cathode.

Layer	Proton (MeV)	Triton (MeV)	^{3}He (MeV)	Alpha (MeV)
Measured by SSB	1.1	1.1	1.1	1.1
6 μm Mylar	0.45	0.55	1.45	1.40
10 μm water	0.53	0.7	1.80	1.80
Total	2.98	2.35	4.35	4.30

at the same time, the discriminator will reject the signal.

As indicated in Table 1, CR-39 detectors used in Pd/D co-deposition experiments showed the presence of energetic charged particles and neutrons [15–18]. To illustrate some of the problems using real-time charged particle detection in electrochemical cells, a Pd/D co-deposition experiment was conducted using a silicon surface barrier detector to detect charged particles in real time. Figure 3a shows a schematic of a cell that was assembled to conduct this measurement. A circular hole was cut into the bottom of the butyrate cell. A 6 μm thick Mylar window was epoxied over the hole using aquarium RTV silicone. Figure 3b shows a schematic of the Au cathode. The Au wires making up the cathode are pressed against the Mylar window. To decrease scattering, a 100 μm thick acrylic collimator, shown in Fig. 3b, was placed on the outside of the cell. The holes cut into the collimator line up with the gold wires. This collimator only allows particles traveling perpendicular to the surface to enter the silicon barrier detector. Once assembled the cell was filled with electrolyte and placed on top of a silicon barrier detector.

Results of the experiments are summarized in Figs. 3c and d. A plot of counts per day for the energy region 1.0–1.5 MeV is shown in Fig. 3c. The arrow indicates when the current was applied to the cell. An increase in the number of counts was observed which immediately dropped down by the next day. This decrease is not surprising. As Pd plates out, the increasing Pd deposit will impede charged particles from reaching the silicon barrier detector. There is also the effect of the Mylar window on the number of observed charged particles. Linear energy transfer (LET) curves indicate that the 6 μm thick Mylar window will cut off <0.45 MeV protons, <0.55 MeV tritons, <1.40 MeV ^{3}He, and <1.45 MeV alphas. Figure 3d is a plot of the count rate on the fourth day divided by the count rate on the third day vs. energy. It is an attempt to characterize the energy of the charged particles observed for the first day of electrolysis. The plot shows that the majority of the charged particles that reached the detector have energies between 1.0 and 2.0 MeV with a peak maximum at 1.1 MeV. To estimate the energy of the energetic charged particles at their birth, it is assumed that they were born near the surface of the Pd and that they transverse through a 10 μm thick water film and a 6 μm thick Mylar film. LET curves were used to determine the energy losses through the water and the Mylar film. The results of these calculations are summarized in Table 2. Because of the experimental configuration used, it was not possible to ascertain the identity of the charged particles.

3. Advantages and Disadvantages of SSNTD

CR-39 is not a relatively new detector material. As indicated vide supra, Cartwright et al [1] were the first to demonstrate that CR-39 could be used to detect nuclear particles in 1978. Since then hundreds of papers in the literature describe the use and development of CR-39 for charged particle detection and neutron dosimetry. Countries involved in this research include Italy [31], Egypt [32,33], India [34], Japan [35], Hungary [36], as well as the United States [1,37]. Landauer uses CR-39 in their Neutrak dosimeter for neutron detection [38]. City University of Hong Kong has a Trackology Research Group headed by Nikezic and Yu [39].

Recently, Durrani [40] wrote a review article discussing the advantages and disadvantages of SSNTDs in detecting energetic particles. Table 3 lists these advantages and disadvantages of SSNTDs as identified by Durrani. SSNTDs do not require a power source nor do they require shielding. They do not generate false signals due to either electronic noise or temperature changes. They are not affected by electromagnetic pulses (EMPs), which is why these detectors

Table 3. Strengths and Weaknesses of SSNTDs [29].

Strengths	Weaknesses
Inexpensive	Lack of real-time capability
Ruggedness and simplicity	Poor charge and energy discrimination-track size/shape depends upon the charge and mass of the particles as well as the angle of incidence. There is significant overlap in the size distributions of the tracks due to energetic particles
Integrating capability	
Responds to both charged particles and neutrons	
Small geometry—trails of damage are nm/μm in diameter and length	Variability in SSNTDs—environmental conditions and manufacturing procedures results in problems of precision and reproducibility
Long history and selectivity of track recording—SSNTDs can retain a record of activity for billions of years	
Existence of thresholds for registration—SSNTDs can register particles only if their charge and LET value are above a threshold	Lack of theoretical understanding—no theoretical work explains how certain properties of materials can predicate or ascertain a viable ability for track formation/retention

are used in the ICF field [3].

It has been shown that the background of CR-39 detectors varies from batch to batch, from foil to foil in the same batch, from one side to another of the same foil and within the same foil surface [41]. Prolonged etching of CR-39 detectors showed that the background track density remains constant once they are fully etched. This indicates that the background is basically due to surface defects. It was also found that the manner in which CR-39 detectors were stored influences the magnitude of the background [42]. When unetched CR-39 detectors were exposed to a neutron source, it was shown that storage at higher temperatures (up to 37°C) resulted in partial or complete removal of tracks [43]. The annealing of damage trails occurs due to diffusion of atomic defects through the crystal lattice or movement of molecular fragments within the polymer. This indicates that, until they are etched, self healing of the detectors will occur with time and that the number of background tracks in the detectors will reach a steady state.

Besides background, there is variability in the response of CR-39 detectors from different vendors to energetic particles. Figure 4a shows the response of CR-39 detectors from TASL [44], Landauer [8], and Fukuvi [8] to different energies of alpha particles. The etching conditions were very similar. It can be seen that the response of Landauer and Fukuvi CR-39 to alpha particles is very similar. However, the alpha tracks obtained using TASL CR-39 are 43% larger than the alpha tracks obtained on either Landauer or Fukuvi CR-39. This is due to the fact that both Landauer and Fukuvi CR-39 have more cross-linking than TASL CR-39. As a result both Landauer and Fukuvi CR-39 are harder than TASL CR-39. The response of Landauer and Fukuvi CR-39 to protons is shown in Fig. 4b. The response to protons overlaps for proton energies greater than 2 MeV but diverges for lower proton energies.

For the electrolysis experiments summarized in Table 1 [10–19], Fukuvi CR-39 was used. Fukuvi brand CR-39 is resistant to chemical damage. This was not true of TASL CR-39. Experiments were conducted using TASL CR-39. An experiment was done in which a Ni screen was placed in contact with a bare TASL CR-39 detector. Electrolysis was then done in a LiCl–H_2O solution for two weeks. Figure 5a shows a photograph of the unetched detector at the end of this experiment. The detector has a frosty appearance except for where the Ni screen was in close contact with it. When this same experiment was done using Fukuvi CR-39, no fogging of the unetched detector was observed. A Pd/D co-deposition experiment was then done on Ag wire in contact with a TASL CR-39 detector. The standard plating/charging protocol was followed [45]. The CR-39 detector was only etched for 2 h. Visual inspection of the

etched detector showed that it had a fogged appearance except for where the cathode had been in close contact with the CR-39. Figure 5b shows a photomicrograph taken at 500× magnification of a cloudy area that was away from the cathode. In the cloudy area, bright, shallow, irregularly shaped features are observed that show no contrast. These features are due to chemical damage of the detector. In the area that had been in contact with the cathode, circular objects are observed that strongly resemble tracks, Fig. 5c. These circular objects are dark on the surface but show bright spots inside when the microscope optics are focused inside the objects. These observations are diagnostic of nuclear generated tracks. A photomicrograph of the interface, Figure 5d, shows the transition from the cloudy area that has been damaged by electrolysis to the area under the cathode. The area damaged by electrolysis shows irregularly shaped features which are distinctly different from the circular shapes observed under the cathode. These experiments demonstrate that not all brands of CR-39 can be used in LENR experiments. The formulation used to fabricate TASL CR-39 detectors makes the detector more sensitive to the detection of energetic particles. However, it also makes TASL detectors more susceptible to chemical damage when used in electrolysis experiments.

One of the most significant advantages of CR-39 for LENR experiments is its integrating capability. Typically emissions occur sporadically or at low fluxes in LENR experiments. For example, Lipson et al. [7], using a NE-213 detector to detect neutrons and a CR-39 detector to detect protons, reported count rates of $(19\pm 2)\times 10^{-3}$ n s^{-1} and $(4\pm 1)\times 10^{-3}$ p s^{-1} in 4π solid angle for their Au/Pd/PdO:H heterostructures. For a CR-39 detector used in a Pd/D co-deposition experiment, Lipson et al. [19] reported count rates of (0.6 ± 0.1) n s^{-1} in 2π solid angle. It would be very difficult to measure such low count rates using real-time detectors. As discussed vide supra, one problem has to do with the solid angle of detection. These issues are eliminated when using a SSNTD. In many of the experiments summarized in Table 1 [10–12, 15–19], the CR-39 detectors were placed in direct contact with the cathode thereby nearly eliminating solid angle detection issues. Because CR-39 is a constantly integrating detector, events are permanently stamped in the plastic. While it will not be known when the events occurred, the signal will not be averaged away and the number of events recorded in the plastic becomes statistically significant. Given the low flux rates and sporadic nature of the emissions, real-time detection can be sacrificed in LENR experiments.

4. Speciation of Energetic Particles Using SSNTD

Another advantage of CR-39 is its ability to speciate energetic particles and neutrons. When a charged particle passes through the plastic, it leaves a trail of damage along its track in the form of broken molecular chains and free radicals. The amount of local damage along the track is related to the local rate at which energy is lost by the particle, dE/dx where x is the distance along the track [46]. Generally, given the bulk etch rate, the first 6 μm of the surface of the CR-

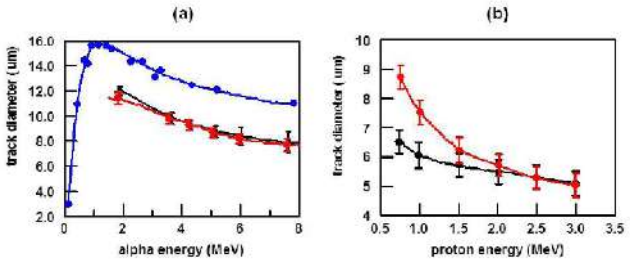

Figure 4. CR-39 calibration curves obtained for (a) alpha particles and (b) protons using TASL (blue), Fukuvi (black) and Landauer (red) CR-39 [8,44]. Fukuvi and Landauer CR-39 detectors were etched in 6 N NaOH solution at 70°C for 7 h. The TASL detector was etched in 7.25 N NaOH solution at 70°C for 7 h.

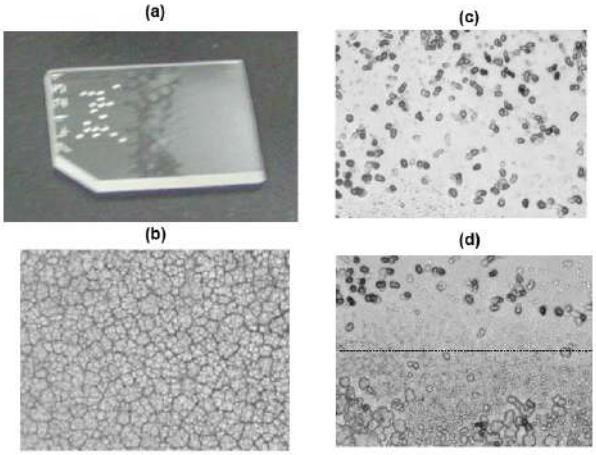

Figure 5. (a) Photograph of a TASL CR-39 detector used in a Ni/H_2O electrolysis experiment. (b–d) Photomicrographs taken at 500X magnification of a TASL CR-39 detector used in a Pd/D co-deposition experiment done on a Ag cathode where (b) was taken in a cloudy area that was not in contact with the cathode, (c) was taken in the area directly under the Ag/Pd cathode, and (d) was taken at the interface (the area above the dotted line was directly underneath the cathode while the area below the dotted line was outside of the cathode).

39 is removed. Any particle, whose LET would stop it within that distance, would not produce a track. This includes particles arriving at oblique angles to the surface. As the particle traverses the CR-39, losing energy, an energetic particle will lose energy along a path dictated by the sine of the entrance angle. Consequently, there is a limit on how oblique the resulting track will be due to LET losses upon entering the CR-39. Furthermore, the track obliqueness provides a means to differentiate between primary charged particles and secondary neutron-induced charged particles. Neutrons interact by either elastic scattering or inelastic interactions with the individual atoms comprising the CR-39. Although these reactions favor forward scattering they are nearly isotropic, resulting in secondary charged particle production over a wide range of angles. Secondary neutron spallation and scattering produces more oblique tracks than primary charged particle.

It turns out that dE/dx is different for different particle types. It is also different for particles of a given type that

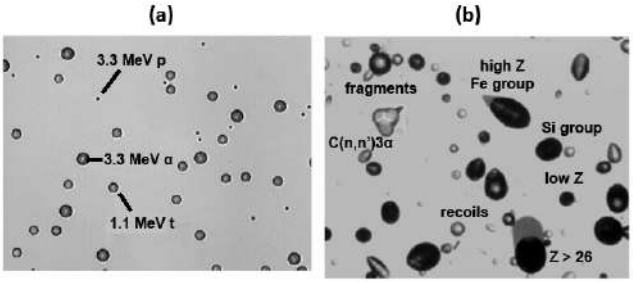

Figure 6. (a) Photomicrograph of CR-39 that was used in an ICF implosion experiment [46]. The detector had been etched for 6 h in 6 M NaOH at 80°C. Republished with permission from the America Institute of Physics. (b) Photomicrograph of a CR-39 detector exposed in the ISS [4]. The detector had been etched for 20 h in 6 M NaOH at 70°C. Republished with permission from Oxford University Press.

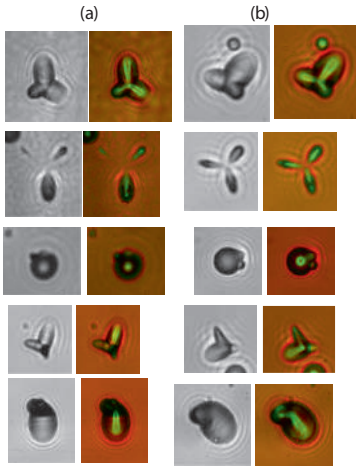

Figure 7. Symmetric triple tracks observed in CR-39 detectors where (a) were generated in Pd/D co-deposition experiments and (b) were generated upon exposure to DT generated neutrons. In both (a) and (b) the left-hand image was obtained with the microscope optics focused on the surface of the CR-39 detector while the right-hand image is an overlay of two photomicrographs taken at different focusing depths (surface of the detector and the bottom of the pits).

have different energies. The diameter of the etched pit provides a measure of dE/dx for the particle. Consequently, diameters can often be used to identify the particle type if the energy is known. Calibration curves, such as those shown in Fig. 4, are used for this purpose. Figure 6a [46] shows tracks obtained as a result of an ICF implosion using D^3He fuel in a thin glass shell. Tracks due to 3.3 MeV protons, 3.3 MeV alphas, and 1.1 MeV tritons are identified. It can be seen that each particle type can be distinguished based on track size. Figure 6b shows tracks obtained on a CR-39 detector inside the International Space Station (ISS) [4]. This detector was part of a stack comprised of three CR-39 sheets. The first and second sheets were separated with 50 μm thick Ti foil. The second and third sheets sandwiched 350 μm Lexan. The stack was wrapped in 30 μm thick Al foil and sealed hermetically in a 40 μm thick polyethylene bag. After etching, the detector shows tracks due to neutron elastic scattering on H, recoil of C and O

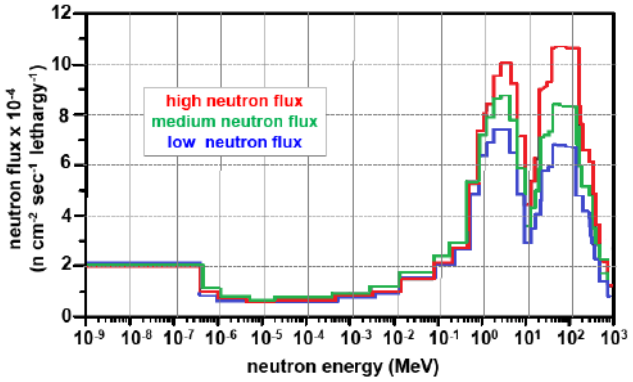

Figure 8. Comparison of neutron energy spectra on three different days as measured by the Bonner ball [48].

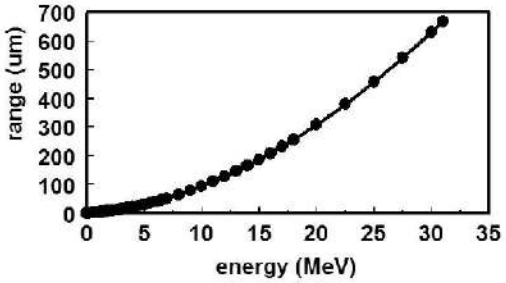

Figure 9. LET curve calculated for alpha particles traversing through CR-39.

atoms, fragmentation, and neutron-induced charged particle reactions including fission. A triple track is seen that is due to the C(n,3a)n' reaction. Additional methods to speciate the charged particle emissions are discussed below.

4.1. Triple tracks

The most easily identified neutron interaction in CR-39 is the carbon break-up reaction. If the energy of a neutron is greater than 9.6 MeV, the inelastic neutron interaction can cause the carbon atom to shatter into three alpha particles. The residuals of the reaction can be viewed in the CR-39 detector as a three-pronged star, or triple track, where each prong represents each charged particle that occurs in the decay. The presence of these triple tracks is diagnostic of >9.6 MeV neutrons.

Roussetski [8] was the first to report seeing triple tracks in his CR-39 detectors that had been placed in contact with Au/Pd/PdO and PdO/Pd/PdO heterostructures that had been loaded electrochemically with D. Once in contact with CR-39, the sample was heated to 50°C to stimulate the desorption of deuterium. The electrolytic loading and thermo-stimulation steps were repeated several times.

Mosier-Boss et al. [17,18] reported seeing triple tracks in CR-39 detectors used in Pd/D co-deposition experiments. Figure 7 shows representative Pd/D co-deposition generated triple tracks as well as their corresponding DT neutron generated triple tracks. Focusing deeper inside the triple tracks, it can be seen that there are three alpha particle generated tracks breaking away from a center point. These features are diagnostic of the carbon breakup reaction. Comparing both sets of triple tracks, it can be seen that the Pd/D co-deposition triple tracks are indistinguishable from the DT neutron generated tracks. The examples of Pd/D and DT neutron tracks do not have the exact same shape. The n $+^{12}$C reaction can proceed to the four-body final state through one or more of the following reaction mechanisms [47]:

$$\mathrm{n} + {}^{12}\mathrm{C} \rightarrow \mathrm{n}' + \alpha + {}^{8}\mathrm{Be} \quad \hookrightarrow 2\alpha \tag{1}$$

$$\mathrm{n} + {}^{12}\mathrm{C} \rightarrow \alpha + {}^{9}\mathrm{Be} \quad \hookrightarrow \mathrm{n}' + {}^{8}\mathrm{Be} \quad \hookrightarrow 2\alpha \tag{2a}$$

$$\mathrm{n} + {}^{12}\mathrm{C} \rightarrow \alpha + {}^{9}\mathrm{Be} \quad \hookrightarrow \alpha + {}^{5}\mathrm{He} \quad \hookrightarrow \mathrm{n}' + \alpha \tag{2b}$$

$$\mathrm{n} + {}^{12}\mathrm{C} \rightarrow {}^{8}\mathrm{Be} + {}^{5}\mathrm{He} \quad \hookrightarrow \mathrm{n}' + \alpha \quad \hookrightarrow 2\alpha \tag{3}$$

$$\mathrm{n} + {}^{12}\mathrm{C} \rightarrow \mathrm{n}' + \alpha + \alpha + \alpha. \tag{4}$$

Processes (1)–(3) are sequential decays going through different excited states of intermediate systems and process (4) is a simultaneous four-body break-up. The observed relative sizes and shapes of the lobes making up the triple tracks in Fig. 7 are the result of these different processes.

No triple tracks have been observed in either control experiments using either $CuCl_2$ or $NiCl_2$ in place of the $PdCl_2$. Nor have they been observed in blank detectors. This indicates that the triple tracks observed in Pd/D co-deposition experiments are not due to cosmic ray spallation neutrons. This is further supported by the cosmic-ray neutron spectrum measured by Nakamura et al. [48], Fig. 8. These spectra were obtained using three neutron detectors, a ^{3}He-loaded multi-moderator detector (Bonner ball), a NE213 organic scintillator, and a high sensitivity rem (dose equivalent) counter. As can be seen in Fig. 8, the energy spectrum of cosmic-ray-induced spallation neutrons consists of three peaks: thermal, 2 MeV evaporation, and a cascade peak at 100 MeV. The thermal and 2 MeV evaporation neutrons will not cause a carbon atom to shatter as the threshold energy for a neutron to cause a carbon atom to shatter is 9.6 MeV. The 100 MeV cascade neutrons will cause a carbon atom to shatter. Energy in the carbon shattering reaction is conserved, where:

$$E_{\mathrm{n}} = E_{\mathrm{th}} + E_{\alpha 1} + E_{\alpha 2} + E_{\alpha 3} + E_{n'}, \tag{5}$$

where E_{n} is the energy of the incoming neutron; E_{th} is the threshold energy required to shatter the carbon atom (9.6 MeV); $E_{\alpha 1}$, $E_{\alpha 2}$, and $E_{\alpha 1}$ are the energies of the alpha particles formed when the carbon atom shatters; and $E_{n'}$ is the energy of the outgoing neutron. If $E_{n'} = 0$ MeV, each alpha particle will have an energy of 30.1 MeV. The LET curve for alpha particles in CR-39, Fig. 9, is used to determine how far these particles will travel through the CR-39 detector. According to the LET curve, 30.1 MeV alphas will travel 635 μm in CR-39. Should a 100 MeV neutron cause a carbon atom to shatter, there will not be a discernible triple track because of the long lengths traveled by the alphas. The residuals of the reaction with a 100 MeV neutron will look like three solitary alpha tracks.

As shown in Fig. 8, the 12–17 MeV neutron energies, which overlaps the energy of DT fusion neutrons, occur an order of magnitude less frequently than either evaporation or cascade neutrons. The total measured background spallation neutron flux was 7.5×10^{-3} n cm^{-2} s^{-1}, with $< 10^{-4}$ n cm^{-2} s^{-1} in the DT fusion neutron energy range.

This low neutron flux, coupled with the CR-39 relative neutron detection inefficiency, $< 10^{-6}$ for triple tracks [37], accounts for the complete absence of triple tracks in the background.

4.2. Fission tracks

Figure 6b shows tracks due to high-*Z* fission fragments. These are examples of fission tracks. As can be seen, the tracks due to these high-*Z* fission fragments are significantly larger than the tracks due to smaller tritons, protons, and alpha particles. The large size of these tracks make them easily identifiable.

Pd/D co-deposition experiments were conducted using uranium as a witness material to determine the energies of the neutrons emitted during the co-deposition process. ^{235}U is fissioned by thermal and higher energy neutrons while ^{238}U is fissioned by >2 MeV neutrons. The cross section for interaction with fast neutrons is equivalent for ^{235}U and ^{238}U, on the order of < 2 barns (as compared to >500 barns for the thermal fission of ^{235}U).

To demonstrate that native uranium isotopes can be fissioned by neutrons, a uranium wire was placed in contact with a CR-39 detector and was exposed to DT neutrons. Afterwards the detector was etched for 1 h. Figure 10a shows a photomicrograph of the etched detector. The arrow indicates a long cylindrical track amongst the oval/circular shaped alpha/neutron recoil tracks. This long cylindrical track is a fission track.

In the Pd/D co-deposition experiment, a 250 μm diamter Au wire was wrapped around a 1 cm length of uranium wire. This composite cathode was placed in contact with a CR-39 detector and Pd/D were electrochemically deposited onto this composite cathode. Figure 10b shows a photomicrograph of tracks observed in the CR-39 detector used in this experiment. Circular and oval alpha tracks due to the decay of uranium and its daughters are observed. Among these alpha tracks, large cylindrical tracks, like the one indicated by an arrow in Fig. 10b, were observed. As shown by the bright streak in the overlay image, this track is shallow. The large track is approximately 40 μm long and 10 μm wide. It is about five times larger than the surrounding alpha tracks and resembles the high-*Z* tracks shown in Fig. 6b and the DT neutron induced uranium fission track shown in Fig. 10a. Such large tracks have not been observed in CR-39 detectors exposed to uranium wire that had not been subjected to Pd/D co-deposition.

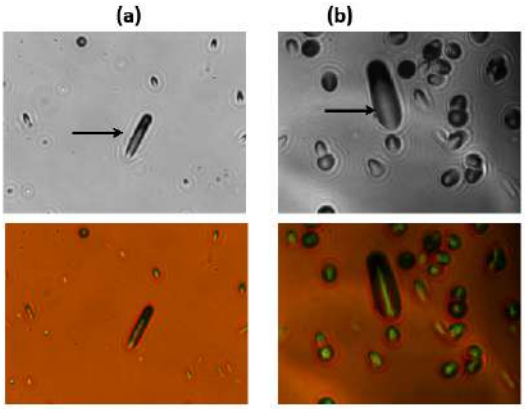

Figure 10. (a) Photomicrographs of a CR-39 detector that had been in contact with uranium wire exposed to DT neutrons. Magnification is 1000×. The detector had been etched for 1 h in 6 M NaOH at 60°C. (b) Photomicrographs of a CR-39 detector that had been used in a Pd/D co-deposition experiment conducted on an Au/U cathode. Magnification is 1000x. The detector had been etched for 6 h in 6 M NaOH at 60°C. The images on the top were obtained with the optics focused on the surface of the detector. The bottom images are an overlay of two images taken at different focusing depths (surface and the bottom of the tracks). Arrows indicate a large elongated track among the uranium alpha tracks.

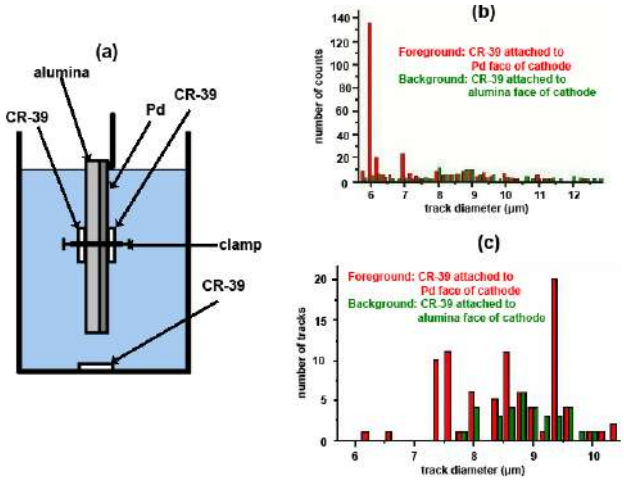

Figure 11. (a) Schematic of the placement of CR-39 detectors used in electrolysis experiments. (b) Number of charged particles vs. track diameter for CR-39 detectors in contact with the thin Pd film cathode and the alumina substrate during electrolysis. (c) Number of charged particles vs. track diameter for CR-39 detectors, shielded with 25 μm Cu film, in contact with the thin Pd film cathode and the alumina substrate during electrolysis.

4.3. The use of shielding films for particle identification

Lipson et al. [11,12,14,49], Karabut et al. [9], and Roussetski et al. [13] have used various foils (11–66 μm thick Al, 25–50 μm thick Cu, and 60 μm thick polyethylene) between the H/D absorbing metal and the CR-39. These shielding foils have known stopping ranges which are used to identify the charged particles.

Figure 11a is a schematic showing the placement of open and shielded CR-39 detectors used in electrolysis experiments [49]. The results using bare and Cu shielded CR-39 detectors are summarized in Fig. 11b and c, respectively. Comparison of track diameters obtained with open and shielded CR-39 allows the identification of charged particles by using the stopping range of the shielding material. A 25 μm Cu film completely absorbs all alpha particles and protons with energies below 9.0 and 2.3 MeV, respectively. For foreground runs (t 2–30 days) with electrolysis of Pd thin film cathodes, the open CR-39 detectors show the appearance of tracks not found in the background detectors in the same electrolysis run. As shown in Fig. 11b, two significant peaks at 6.0 and 7.0 μm are observed. For shielded CR-39 detectors (25 μm Cu film) using the same cathode, the 6 μm peak of the open CR-39 disappears due to the Cu shielding, Fig. 11c. The disappearance of the 6.0 μm peak in the Cu shielded detector indicates that this peak is due to low MeV protons. From calibration data, the proton energy was estimated to be 1.5–1.7 MeV. The 7.0 μm peak in the open CR-39, Fig. 11b, shifts to larger track diameters and splits into three narrow peaks, Fig. 11c. Due to its shift and splitting after crossing the Cu shield, the 7.0 μm peak in Fig. 11b is attributed to α-particles with energies between 11.0 and 16.0 MeV.

4.4. Successive (or sequential) etching for particle identification

Lipson and Roussetski [19] developed a successive etching technique to identify the charged particles and their energies responsible for the tracks in CR-39 detectors. This successive etching method has been used by other groups working with radioactive materials to identify and determine the energies of emitted charged particles [50–53]. In this approach, calibration curves were generated by exposing CR-39 detectors to alpha particles and protons of known energies. Lipson et al. exposed CR-39 detectors to alpha sources with energies in the range of 1.6–7.7 MeV and to monoenergetic

cyclotron alpha-beams in the energy range of 10–30 MeV. Detectors were also calibrated with Van de Graff accelerator producing monoenergetic proton beams with energy ranges of 0.75–3 MeV. Only circular tracks are used to generate calibration curves. These tracks are created by charged particles with trajectories normal to the surface of the detector. There is an inverse relationship between the charged particle energy and the track diameter. The smaller the diameter, the higher the energy. There is also a cutoff in energy that will result in a track. Figure 12a and b show alpha and proton calibration curves, respectively, after 7, 14, 21, and 28 h of etching. As can be seen from these calibration curves, alpha particles with energies less than 6 MeV and protons with energies less than 1 MeV can be identified after a 7 h etch time. However, longer etching times are required to unambiguously identify alphas and protons energies greater than 6 MeV and 1 MeV, respectively.

SRI conducted several Pd/D co-deposition experiments that used CR-39 detectors. The experiments were conducted in the presence of a magnetic field. Two experiments were done with the detector inside the cell. In these experiments a 60 μm thick polyethylene film separated the Ag cathode from the detector. These detectors, identified

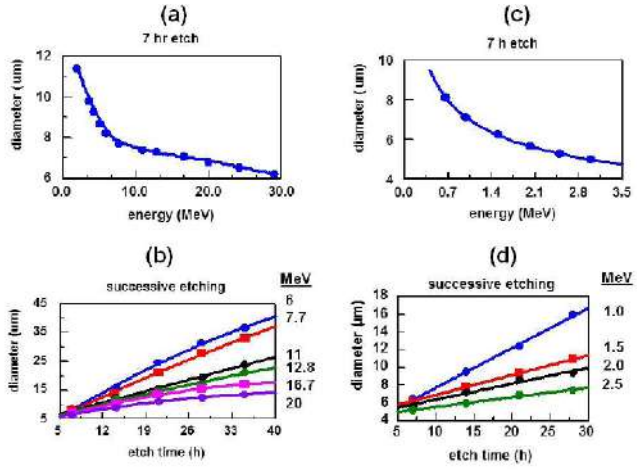

Figure 12. Calibration curves generated for energetic alpha and proton particles. (a) Alpha track size as a function of energy (7 h etch). (b) Track diameter vs. etching time for six different alpha energies. Alpha particle energies are indicated. (c) Proton track size as a function of energy (7 h etch). (b) Track diameter vs. etching time for four different proton energies. Proton energies are indicated.

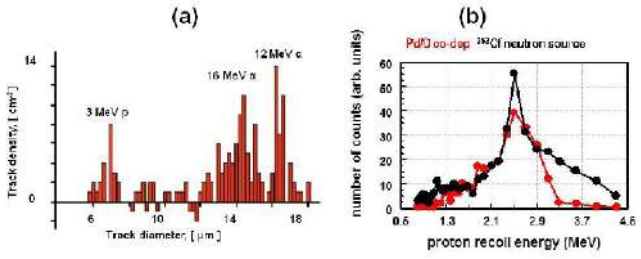

Figure 13. Results obtained for the sequential etching. (a) The front side spectrum of nuclear tracks in detector 10-5 after subtracting the neutron induced proton recoil spectrum from its back side (etch time is 21 h). (b) Reconstruction of the proton recoil spectra for detector 10-7 and a detector exposed to ^{252}Cf neutrons (etch time 14 h).

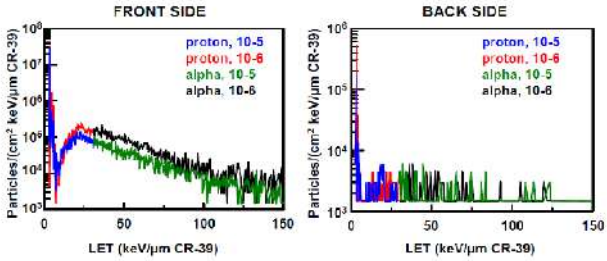

Figure 14. LET spectra of differential fluence calculated for the front and back surfaces of detectors 10-5 and 10-6. The front surface was the side closest to the cathode.

as 10-5 and 10-6, underwent successive etching analysis by Lipson and Roussetski. Using this process, they identified 3 MeV protons, 16 MeV alphas, and 12 MeV alphas in the CR-39 detectors used in heavy water experiments, Fig. 13a. No tracks above background were observed in the light water experiments. In another SRI experiment, the CR-39 detector was placed outside the cell. A 6 μm thick Mylar film was placed between the detector and the Ag cathode. The detector used in this experiment also underwent successive etching analysis by Lipson and Roussetski. In their analysis, they identified proton recoil tracks due to 2.45 MeV (DD) neutrons, Fig. 13b.

4.5. LET spectrum analysis for particle identification

The CR-39 detectors used in the SRI immersion experiments, detectors 10-5 and 10-6, were scanned using an automated scanning track analysis system to obtain quantitative information on the pits produced in the CR-39. The scanner has a high quality microscope optical system operating at a magnification high enough to discriminate between tracks and background. The images obtained were analyzed by the proprietary software that made 15 characteristic measurements of each feature located in the image. These measurements were used to reliably discriminate between etched tracks and background features present on and in the plastic detector.

Zhou, of NASA-Johnson Space Center, took the scanned data of detectors 10-5 and 10-6 and analyzed them using a LET spectrum method [54–59]. In this analysis, Zhou used the scanned values of the major and minor axes of the tracks to differentiate the charged particle species and energy. Applying the LET spectrum method, differential/integral fluence, Fig. 14, and the energy distributions of the charged particles, Fig. 15, were determined. For protons, a the major peak is observed at $11.5 - 12$ MeV for the front CR-39 surfaces and 9.75 MeV for the back CR-39 surfaces.

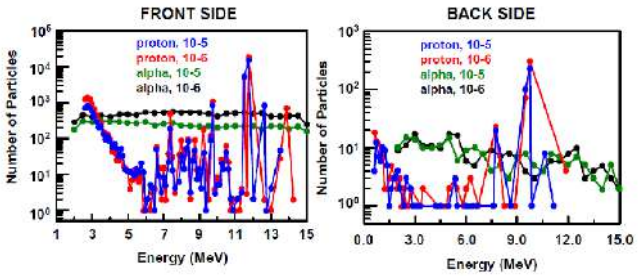

Figure 15. Energy distribution of particles calculated for the front and back surfaces of detectors 10-5 and 10-6. The front surface was the side closest to the cathode.

The distribution of a particles is nearly uniform because they are mainly secondary particles.

5. Conclusions

Compared to electronic, real-time detectors, solid state nuclear track detectors, such as CR-39, are ideal for use in LENR experiments. The advantages of CR-39 over real-time, electronic detectors are:

(1) CR-39 detectors do not require power and can be placed in close proximity to the cathode. This eliminates the solid angle detection losses.
(2) CR-39 detectors can be used in both electrolysis and gas loading experiments.
(3) CR-39 detectors are not affected by low level electronic noise from the local environment and do not require shielding. Nor do they respond to temperature changes.
(4) CR-39 is an example of a constantly integrating detector. When an event occurs it is permanently stamped in the plastic. Nothing gets averaged away. This is important for reactions that occur sporadically in bursts or at low flux levels, which is often true of LENR experiments.
(5) The size and shape of the tracks in CR-39 detectors can be used to identify the energetic particles that caused them.
(6) CR-39 detectors are robust and inexpensive.
(7) CR-39 detectors retain their record of nuclear activity for decades and can be repeatedly re-examined.
(8) Real-time electronic detectors require expensive and complicated electronic modules that are required for both timing and background discrimination, even if shielding is present. Unlike CR-39, electronic, real-time detectors tend to discriminate against multiple simultaneous events. This results in an undercounting of the nuclear products.

Given all these advantages over electronic, real-time detectors, solid state nuclear track detectors, such as CR-39, are the detector of choice in LENR experiments.

Acknowledgements

This work was funded by the Defense Threat Reduction Agency (DTRA), and JWK Corporation. The authors would like to thank Dr. Gary Phillips, nuclear physicist, retired from the Naval Research Laboratory, US Navy, Radiation Effects Branch for valuable discussions on CR-39. They would also like to thank Dr. Roger Boss for doing the probability analysis of the bubble detectors. The authors would also like to thank Mr. Mark Morey, Dr. Jim Tinsley, and Mr. Paul Hurley of National Security Technologies, LLC, Special Technologies Laboratory in Santa Barbara, CA for exposing CR-39 detectors to DT neutrons. Finally, the authors would like to thank Dr. Frank Gordon, retired Head of Research and Applied Sciences Dept. SSC-Pacific, for all the support he had provided in this field of research.

References

[1] B.G. Cartwright, E.K. Shirk and P.B. Price, A nuclear-track recording polymer of unique sensitivity and resolution, *Nucl. Instrum. Meth.* **153** (1978) 457–460.
[2] D. Nikezic and K.N. Yu, Formation and growth of tracks in nuclear track materials, *Mater. Sci. Eng. R* **46** (2004) 51–123.
[3] J.A. Frenje, C.K. Li, F.H. Séguin, D.G. Hicks, S. Kurebayashi, R. D. Petrasso, S. Roberts, V. Yu. Glebov, D.D. Meyerhofer, T.C. Sangster, J.M. Soures, C. Stoeckl, C. Chiritescu, G.J. Schmid and R.A. Lerche, Absolute measurements of neutron yields from DD and DT implosions at the OMEGA laser facility using CR-39 track detectors, *Rev. Sci. Instrum.* **73** (2002) 2597–2606.

[4] J.K. Pálfalvi, Y. Akatov, J. Szabó, L. Sajó-Bohus and I. Eördögh, Evaluation of solid state nuclear track detector stacks exposed on the international space station, *Radiat. Prot. Dosimetry* **110** (2004) 393–397.
[5] X.-Z. Li, D.-W. Mo, L. Zhang, S.-C. Wang, T.-S. Kang, S.J. Liu and J. Wang, Anomalous nuclear phenomena and solid state track detector, *Nucl. Tracks and Rad. Meas.* **22** (1993) 599–604.
[6] S. Jin, F. Zhan and Y. Liu, Deuterium absorbability and anomalous nuclear effect of YBCO high temperature superconductor, *Proc. Fourth Int. Conf. on Cold Fusion*, Vol. 3, Nuclear Measurements Papers, Lahaina, Maui, Hawaii, Dec. 6Ű9, 1993, T.O. Passell (Ed.), Electric Power Research Institute, Palo Alto, CA, 1994, pp. 4.1–4.3.
[7] A. Lipson, F. Lyakhov, A. Roussetski, T. Akimoto, N. Asami, R. Shimada, S. Miyashita and A. Takahashi, Eevidence for low-intensity D-ŰD reaction as a result of exothermic deuterium desorption from Au/Pd/PdO:D heterostructure, *Fusion Sci. Techno. 38* (2000) 238–252.
[8] A.S. Roussetski, Application of CR-39 plastic track detector for detection of DD and DT-reaction products in cold fusion experiments, *Proc. 8th Int. Conf. on Cold Fusion*, May 21Ű-26, 2000, Lerici (La Spezia), Italy, Italian Physical Society, Bologna, Italy.
[9] A.G. Lipson, A.B. Karabut and A.S. Roussetsky, Anomalous enhancement of DD-reaction, alpha emission and X-ray generation in the high current pulsing deuterium glow-discharge with Ti-cathode at the voltages ranging from 0.8 to 2.5 kV, *Proc. 9th Int. Conf. on Cold Fusion*, 2002, Beijing, China.
[10] R.A. Oriani and F.C. Fisher, Generation of nuclear tracks during electrolysis, *Jpn. J. Appl. Phys.* **41** (2002) 6180–6182.
[11] A.G. Lipson, A.S. Roussetski, G.H. Miley and C.H. Castano, In-situ charged particles and X-ray detection in Pd thin ?lm cathodes during electrolysis in Li2SO4/H2O, in Condensed Matter Nuclear Science: Proceedings of the 9th International Conference on Cold Fusion, Beijing, China, May 19Ű24, 2002; X.Z. Li (Ed.), Tsinghua Univ. Press, Beijing, 2002, pp. 218–223.
[12] A.G. Lipson, A.S. Roussetski, G.H. Miley and E.I. Saunin, Phenomenon of an energetic charged particle emission from hydrogen/deuterium loaded metals, In Condensed Matter Nuclear Science: Proceedings of the 10th International Conference on Cold Fusion, Cambridge, MA, Aug. 24Ű29, 2003, P.L. Hagelstein and S.R. Chubb (Eds.), World Scientific, Singapore, 2006, pp. 539–558.
[13] A.S. Roussetski, A.G. Lipson and V.P. Andeanov, Nuclear emissions from titanium hydride/deteride induced by powerful picoseconds laser beam, In Condensed Matter Nuclear Science: Proceedings of the 10th International Conference on Cold Fusion, Cambridge, MA, Aug. 24Ű29, 2003, P.L. Hagelstein and S.R. Chubb (Eds.), World Scientific, Singapore, 2006, 559–566.
[14] A. Lipson, I. Chernov, A. Roussetski, Y. Cherdantsev, A. Tsivadze, B. Lyakhov, E. Saunin and M. Melich, Hot deuteron generation and charged particle emissions on excitation of deuterium subsystem in metal deuterides, Low-Energy Nuclear Reactions Sourcebook Volume 2, J. Marwan and S. Krivit (Eds,), American Chemical Society, Washington, DC, 2009, 95–117.
[15] P.A. Mosier-Boss, S. Szpak, F. Gordon and L. Forsley, Use of CR-39 in Pd/D Co-deposition experiments, Eur. Phys. J. Appl. Phys. 40 (2007) 293Ű303.
[16] P.A. Mosier-Boss, S. Szpak, F. Gordon and L. Forsley, Characterization of tracks in CR-39 detectors obtained as a result of Pd/D Co-deposition, Eur. Phys. J. Appl. Phys. 46 (2009) 309001 1–12.
[17] P.A. Mosier-Boss, S. Szpak, F. Gordon and L. Forsley, Triple tracks in CR-39 as the result of Pd–D Co-deposition: evidence of energetic neutrons, Naturwissenschaften 96 (2009) 135–142.
[18] P.A. Mosier-Boss, J.Y. Dea, L.P.G. Forsley, M.S. Morey, J.R. Tinsley, J.P. Hurley and F.E. Gordon, Comparison of Pd/D co-deposition and DT neutron generated triple tracks observed in CR-39 detectors, Eur. Phys. J. Appl. Phys. 51 (2010) 20901–1–10.
[19] A.G. Lipson, A.S. Roussetski, E.I. Saunin, F. Tanzella, B. Earle and M. McKubre, Analysis of the CR-39 detectors from SRIŠs SPAWAR/Galileo type electrolysis experiments # 7 and # 5. Signature of possible neutron emission, Proceedings of 8th International Workshop on Anomalies in Hydrogen/Deuterium Loaded Metals, J. Rothwell and P. Mobberley (Eds), International Society for Condensed Matter Nucleus Science, 2008, 182–203.
[20] P.K. Iyengar and M. Srinivasan, BARC Studies In Cold Fusion, BARC-1500. Government of India, Atomic Energy Commission: Bombay (1989).
[21] A. De Ninno, et al., Emission of neutrons as a consequence of titanium-deuterium interaction. Nuovo Cimento Soc. Ital. Fis.

A, 101 (1989) 841.
[22] A. De Ninno, A. Frattolillo, G. Lollobattista, L. Martinis, M. Martone, L. Mori, S. Podda and F. Scaramuzzi, Evidence of emission of neutrons from a titanium-deuterium system, Europhys. Lett., 9 (1989) 221–224.
[23] E. Jones, F.W. Keeney, A.C. Johnson, D.B. Buehler, F.E. Cecil, G. Hubler, P.L. Hagelstein, J.E. Ellsworth and M.R. Scott, Neutron emissions from metal deuterides, In Condensed Matter Nuclear Science: Proceedings of the 10th International Conference on Cold Fusion, Cambridge, MA, Aug. 24Ű29, 2003, P.L. Hagelstein and S.R. Chubb (Eds.), World Scientific, Singapore, 2006, 525–533.
[24] A. Shyam and R.K. Rout, Observation of neutrons from palladium deuteride X pinches using a simple low energy capacitor bank, IEEE Transactions on plasma science 27 (1999) 1210–1213.
[25] T.N. Claytor, M.J. Schwab, D.J. Thoma, D.F. Teter and D.G. Tuggle, Tritium production from palladium alloys, The 7th International Conference on Cold Fusion, 1998. Vancouver, Canada; ENECO, Inc., Salt Lake City, UT, p. 88.
[26] R. Taniguchi, T. Yamamoto and S. Irie, Detection of charged particles emitted by electrolytically induced cold nuclear fusion, Jpn. J. Appl. Phys. 28 (1989) L2021–L2023.
[27] A.G. Lipson, B.F. Lyakhov, A.S. Roussetsky and N. Asami, Evidence for DD-reaction and a long-range alpha emission in Au/Pd/PdO:D heterostructures as a result of exothermic deuterium desorption, Proc. 8th Int. Conf. on Cold Fusion, May 21Ű26, 2000, Lerici (La Spezia), Italy, Italian Physical Society, Bologna, Italy.
[28] S.E. Jones, F.W. Keeney, A.C. Johnson, D.B. Buehler, F.E. Cecil, G. Hubler, P.L. Hagelstein, J.E. Ellsworth and M.R. Scott, Charged-particle emissions from metal deuterides, In Condensed Matter Nuclear Science: Proceedings of the 10th International Conference on Cold Fusion, Cambridge, MA, Aug. 24Ű29, 2003, P.L. Hagelstein and S.R. Chubb (Eds.), World Scientific, Singapore, 2006, 509–523.
[29] J.F. Ziegler, J.P. Biersack, The Stopping and Range of Ions in Solids, Pergamon Press, NewYork (1985).
[30] S.E. Jones, D.E. Jones, D.S. Shelton, S.F. Taylor, Search for neutron, gamma and x-ray emissions From Pd/LiOD electrolytic cells: a null result, Trans. Fus. Technol. 8 (1994) 143.
[31] E.Vilela, E. Fantuzzi, G. Giacomelli, M. Giorgini, B. Morelli, L. Patrizii, P. Serra and V. Togo, Optimization of CR-39 for fast neutron dosimetry applications, Rad. Meas. 31 (1999) 437–442.
[32] A.R. El-Sersy, N.E. Khaled and S.A. Eman, Determination of CR-39 detection efficiency for fast neutron registration and the absolute neutron dosimetry, Nucl. Instr. and Meth.in Phys. Res. B 215 (2004) 443–448.
[33] A.R. El-Sersy, Study of absolute fast neutron dosimetry using CR-39 track detectors, Nucl. Instr. and Meth.in Phys. Res. A 618 (2010) 234–238.
[34] V. Kumar, R.G. Sonkawade and A.S. Dhaliwal, Optimization of CR-39 as neutron dosimeter, Ind. J. of Pure and Appl. Phys. 48 (2010) 466–469.
[35] T. Tsuruta, T. Niwa and Y. Fukumoto, Experimental, study of CR-39 etched track detector for fast neutron dosimetry, J. Nucl. Sci. and Technol. 29 (1992) 1108– 1115.
[36] J.K. Pálfalvi, J. Szabó, Yu. Akatov, L. Sajó-Bohus and I. Eördögh, Cosmic ray studies on the ISS using SSNTD, BRADOS projects, 2001–2003, Radiat. Meas. 40 (2005) 428–432.
[37] G.W. Phillips, J.E. Spann, J.S. Bogard, T. VoDinh, D. Emfietzoglou, R.T. Devine and M. Moscovitch, Neutron spectrometry using CR-39 track etch detectors, Radiat. Prot. Dosim. 120 (2006) 457–460.
[38] http://www.landauerinc.com/uploadedFiles/Healthcare_and_Education/Products/Dosimeters/ Neutrak%20Specifications.pdf
[39] http://www.cityu.edu.hk/ap/nru/nrures_t.htm
[40] S.A. Durrani, Nuclear Tracks today: strengths, weaknesses, challenges, Rad. Measurements 43 (2008) S26ŰS33.
[41] R. Mishra, C. Orlando, L. Tommasino, S. Tonnarini and R. Trevisi, A better understanding of the background of CR-39 detectors, Radiat. Meas. 40 (2005) 325–328.
[42] N. Ishigure and O. Matsuika, Evaluation of background in CR-39 detector for a-particle detection, Hoken Butsuri 22 (1987) 287–293.
[43] N.A. Al-Liabi, The effects of storage on CR-39, Isotopenpraxis 27 (1991) 56–57.
[44] C. Brun, M. Fromm, M. Jouffroy, P. Meyer, J.E. Groetz, F. Abel, A, Chambaudet, B. Dörschel, D. Hermsdorf, R. Bretschneider, K. Kadner and H. Kühne, Intercomparative study of the detection characteristics if the CR-39 SSNTD for light ions: present status of the besancon-dresden approaches, Radiat. Meas. 31 (1999) 89–98.
[45] http://newenergytimes.com/v2/projects/tgp/Welcome.shtml

[46] F.H. Séguinm J.A. Frenje, C.K. Li, D.G. Hicks, S. Kurebayashi, J.R. Rygg, B.-E. Schwartz, R.D. Petrasso, S. Roberts, J.M. Soures, D.D. Meyerhofer, T.C. Sangster, J.P. Knauer, C. Sorce, V. Yu Glebov, C. Stoeckl, T.W. Phillips, R.J. Leeper, K. Fletcher and S. Padalino, Spectrometry of charged particles from inertial-confinement-fusion plasmas, Rev. Sci. Instrum. 74 (2003) 975–995.

[47] B. Antolkovic and Z. Dolenec, The neutron-induced 12C(n,n')3a reaction at 14.4 MeV in a kinematically complete experiment, Nucl. Phys. A 237 (1975) 235–252.

[48] T. Nakamura, T. Nunomiya, S. Abe, K. Terunuma and H. Suzuki, Sequential measurements of cosmic-ray neutron spectrum and dose rate at sea level in Sendai, Japan, J. Nucl. Sci. and Technol. 42 (2005) 843–853.

[49] A.G. Lipson, G.H. Miley, A.S. Roussetski and E.I. Saunin, Phenomenon of an energetic charged particle emission from hydrogen/deuterium loaded metals, In Condensed Matter Nuclear Science: Proceedings of the 10th International Conference on Cold Fusion, Cambridge, MA, Aug. 24Ű29, 2003, P.L. Hagelstein and S.R. Chubb (Eds.), World Scientific, Singapore, 2006, 539–558.

[50] A,K, Pandey, R.C. Sharma, P.C. Kalsi, R.H. Iyer, Measurement of alpha to fission branching ratios of heavy actinides by sequential etching of alpha and fission tracks in CR-39, Nucl. Instru. and Meth. in Phys. Res. B, 82 (1993) 151–155.

[51] D. Paul, D. Ghose, R.C. Sastri, An SSNTD study of spontaneous fission fragments from the soil-gas samples of Bakreswar thermal springs, Rad. Meas., 33 (2001) 167–169.

[52] M. Luszik-Bhadra, F. dErrico, L. Lusini, B. Wiegel, Microdosimetric investigations in a proton therapy beam with sequentially etched CR-39 track detectors, Rad. Prot. Dosim., 66 (1996) 353–358.

[53] M. Fromm, F. Membrey, A. El Rahamany, A. Chambaudet, Principle of light ions micromapping and dosimetry using a CR-39 polymeric detector: modelized and experimental uncertainties, Nucl. Tracks and Rad. Meas., 21 (1993) 357–365.

[54] D. OŠSullivan, D. Zhou, W. Heinrich, S. Roesler, J. Donnelly, R. Keegan, E. Flood and L. Tommasino, Cosmic rays and dosimetry at aviation altitudes, Radiat. Meas., 31 (1999) 579–584.

[55] D. OŠSullivan, D. Zhou, E. Semones, W. Heinrich and E. Flood, Dose equivalent, absorbed dose and charge spectrum investigations in low earth orbit, Adv. Space Res., 34 (2004) 1420–1423.

[56] D. Zhou, E. Semones, R. Gaza, S. Johnson, N. Zapp and M. Weyland, Radiation measured ISS-expedition 12 with different dosimeters, Nucl. Instr. Meth., A580 (2007) 1283–1289.

[57] D. Zhou, E. Semones, R. Gaza, S. Johnson, N. Zapp, M. Weyland, R. Rutledge and T. Lin, Radiation measured with different dosimeters during STS-121 space mission, Acta Astron., 64 (2009) 437–447.

[58] D. Zhou, E. Semones, R. Gaza, S. Johnson, N. Zapp, K. Lee and T. George, Radiation measured during ISS-expedition 13 with different dosimeters, Adv. Space Res., 43 (2009) 1212–1219.

[59] D. Zhou, E. Semones, D. OŠSullivan, N. Zapp, M. Weyland, G. Reitz, T. Berger and E.R. Benton, Radiation measured for MATROSHKA-1 experiment with passive dosimeters, Acta Astron., 66 (2010) 301–308.